Journal of Colloid and Interface Science 612 (2022) 261–266

Contents lists available at ScienceDirect

Journal of Colloid and Interface Science

journal homepage: www.elsevier.com/locate/jcis

Interfacial instabilities in Marangoni-driven spreading of polymer solutions on soap films

Melika Motaghian *, Thiemo van Esbroeck, Erik van der Linden, Mehdi Habibi *

Physics and Physical Chemistry of Foods, Wageningen University, Wageningen 6708 WG, The Netherlands

GRAPHICAL ABSTRACT

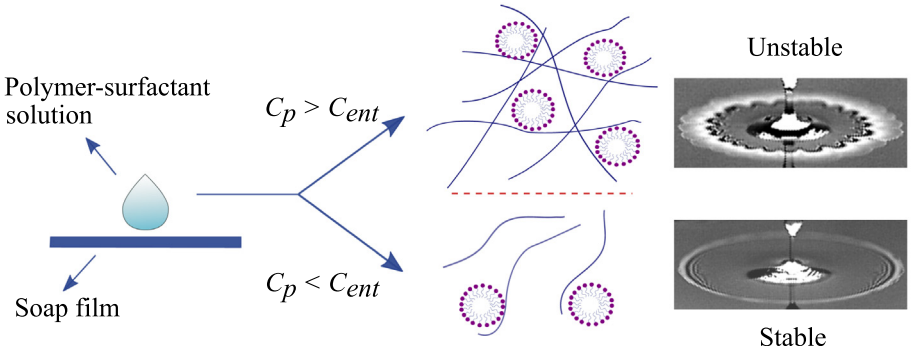

ARTICLE INFO

Article history:
Received 2 November 2021
Revised 23 December 2021
Accepted 24 December 2021
Available online 29 December 2021

Keywords:
Interfacial flow
Instability
Marangoni spreading
Polymers
Surfactants

ABSTRACT

Hypothesis: Tuning and controlling the flow behavior of multi-component liquids has been a long-lasting struggle in various technological applications. Here, we studied Marangoni spreading of a polymer-surfactant ternary solution when deposited on a soap film with higher surface tension. The spreading front becomes unstable into a fingering pattern above the entanglement concentration of the polymer solution, indicating that the interplay between the elastic and interfacial properties drives the instability. Balancing these terms results in a critical length scale for the onset of the instability.

Experiments: To investigate the connection between the rheological characteristics of the samples and the origins of the instabilities, various rheological tests were performed. Elastic and loss modulus of the samples were measured within the linear viscoelastic regime. The spreading behavior of the solutions was studied using high-speed imaging techniques.

Findings: At low concentrations of polymers, spreading dynamics are governed by surface tension gradient and viscous dissipation leading to a stable front growing linearly in time. However, above the entanglement concentration of polymers spreading front destabilizes into a daisy shape pattern suggesting the elastic forces dominating the spreading dynamics. We introduced a length scale that precisely predicts the onset of the instability.

1. Introduction

Spreading of a droplet over a solid or liquid surface is a sophisticated and omnipresent phenomenon in various fields of science and technology [1,2]. Ink-jet printing, spray coating, cleaning sili-

* Corresponding authors.
E-mail addresses: Melika.motaghian@wur.nl (M. Motaghian), Mehdi.habibi@wur.nl (M. Habibi).

https://doi.org/10.1016/j.jcis.2021.12.168
0021-9797/

con wafers [3] and many other industrial applications rely majorly on the spreading behavior of liquids [4]. During spreading, a complex interplay takes place between surface tension gradients, viscous and inertial forces, leading to perplexing dynamics [5]. Moreover, boundary conditions and, in particular, high shear forces caused by solid boundaries dictate dramatic changes in the flow profile [6], especially in non-Newtonian fluids. To simplify the problem, previous studies have mainly focused on the spreading of single-component liquids or solutions with very low concentrations of polymer [7], often in the vicinity of a solid boundary. Thus physical aspects of the spreading of multicomponent droplets in the absence of the no-slip boundary condition have not been fully captured yet. However, free-surface flows are widespread in the industry, and fluids are often multi-component, containing polymers and surface-active molecules. Microscopic interactions between these molecules can dramatically influence the flow behavior of the whole solution [8,9] and, in many cases, lead to instabilities [10–12]. Fragmentation [13–15], formation of beads, blisters [16,17], or large terminal drops [18] during the breakup of a polymer solution are instances of these instabilities. They are often undesired; therefore, a complete understanding of the dynamics of these instabilities is required to tune the flow and impede the instabilities.

In this study, we unravel a novel instability in the spreading of multi-component droplets containing high molecular weight polymer and surfactant on a thin soap film. When a droplet is deposited on a soap film, depending on its surface tension, it can spread and form a new film in the center of the soap film [19]. This unique geometry allows studying the spreading behavior in the absence of high shear viscous forces induced by the no-slip boundary condition. We observe that at relatively low polymer concentration, spreading takes place smoothly, and the leading edge remains perfectly circular. However, above a critical concentration (C_l), the spreading front is no longer stable. Undulations emerge at the front line and form a daisy shape pattern. Fig. 1 (top row) shows the spreading front of two droplets below (left) and above (right) C_l.

We first discuss the experimental procedure, including the rheological characterization of our polymer-surfactant ternary solutions and the spreading dynamics. Then we continue with introducing the instability and the triggering parameters related to the critical concentration of polymers. We provide a scaling argument that predicts the onset of the instability.

2. Experimental procedure

Polymer-surfactant solutions were prepared by slowly adding powdered polymer to the mixture of surfactant and Milli-Q water. Then they were placed on a rotator at low rotating speed for a day to ensure that mixing was homogenous and polymer chains were not broken due to the high shear rates of mixing flows. We studied various combinations of polymers and surfactants, including polyethylene oxide (PEO) different molecular weight (0.3 - 4 $\times$ 10^6 amu, 99%, Sigma Aldrich), polyacrylamide (PAM, Mw $\sim$ 18 $\times$ 10^6, 99%, Sigma Aldrich), sodium dodecyl sulfate (SDS, 98%, Sigma Aldrich), ammonium lauryl sulfate (ALS, 30% in H_2O, Sigma Aldrich), and dioctyl sulfosuccinate sodium salt (AOT, 97%, Sigma Aldrich). We use solutions of PEO 4 $\times$ 10^6 amu and 0.3 M SDS as an explanatory case; some details on the rest of the solutions can be found in SI.

Rheological properties of the solutions were studied using a stress-controlled rheometer (MCR 302, Anton Paar) equipped with a cone-plate geometry (diameter of 50 mm and angel of 4°). Shear viscosity of the samples was measured within the shear rates of 0.01 to 1000 1/s.

Amplitude sweep tests were performed on the solutions with the lowest and highest polymer concentration to determine the linear viscoelastic region (LVE). 10% strain was then selected within LVE to perform the frequency sweep tests.

In order to measure the surface tension of the samples in a time scale relevant to that of the spreading experiments, we used Krüss BPT Mobile bubble pressure surface tensiometer. With this method, the dynamic surface tension of the solutions was measured in time scales as short as 10 ms. For highly concentrated samples, however, reaching10 ms time scale was not feasible due to the very high viscosity of the solution.

After characterization of the samples, droplets of polymer-surfactant solutions were gently deposited on a soap film of 0.01 M SDS. The following spreading was recorded with a Phantom

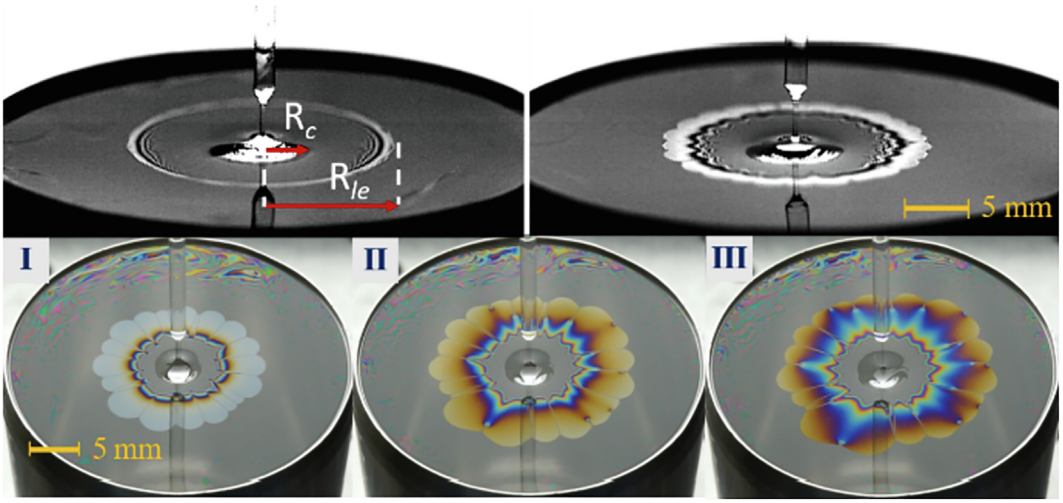

Fig. 1. (Top row) Droplets of PEO-SDS solution spread on soap films of 0.01 M SDS. Both droplets contain 0.3 M SDS. Concentrations of PEO (Mw $\sim$ 2 $\times$ 10^6) solutions are 4 gr/L (left) and 14 gr/L (right). Above the critical concentration (right), the leading edge destabilizes into a daisy shape pattern. (Bottom row) Colored images of the unstable spreading front of PEO 12 gr/L. Images are 500 ms apart. The thickness of the advancing region is in the order of the wavelength of visible light and changes in the film thickness cause the rainbow patterns.

high-speed camera (V710) at 4000f/s. These video frames were image processed to track the radius of the spreading regions in time.

3. Results and discussion

3.1. Rheological characterization

Microscopic interactions between polymer strands can heavily influence the rheological properties of a polymer solution. Increasing the concentration highly promotes these interactions and, therefore causes different topological state transitions [20,21] such as non-entangled to entangled polymeric phase. The footprint of these phase transitions can be found in the rheological properties of the solution [22,23]. One approach is to study the shear viscosity of the solutions as the polymer concentration increases. In Fig. 2 shear viscosity of the samples containing 0.3 M SDS and different concentrations of PEO is presented. All the samples showed a clear shear thinning behavior within the shear rates of 0.01 to 1000 1/s which became more pronounced with the increment of polymer concentration.

Carreau-Yassuda model was fitted to the data sets to extract the zero shear viscosity (η_0). In Fig. 3, η_0 is presented for different concentrations of PEO of three different molecular weights (3×10^5, 2×10^6, and 4×10^6 amu) and polyacrylamide (PAM) with a molecular weight of 18×10^6 amu. The concentration range in all of our polymer-SDS solutions is above c + and the solutions are in a semi-dilute regime. Therefore, the change in the slope of the lines in Fig. 3 indicates the transition from non-entangled to entangled polymeric states.

According to Fig. 3, the entanglement concentration (Ce) determined from the crossover concentration is 50, 8, and 7 gr/L for PEO 3×10^5 2×10^6, and 4×10^6 amu, respectively. For PAM 18×10^6 the pivot point occurs at 5gr/L. As it can be seen, by increasing the molecular weight of the polymer, the entanglement occurs at lower concentrations.

To characterize the viscoelastic properties of the samples, frequency sweep tests were performed within the linear viscoelastic regime. Elastic (G') and loss (G'') modulus of the PEO (4×10^6 amu) solutions are presented In Fig. 4. By increasing the concentration of polymer, both G' and G'' of the samples increased. As it is known for polymer solutions, at low frequencies, the loss modulus (G'') of all samples was larger than the respective elastic modulus (G') and by increasing the frequency, G' grew and surpassed G''.

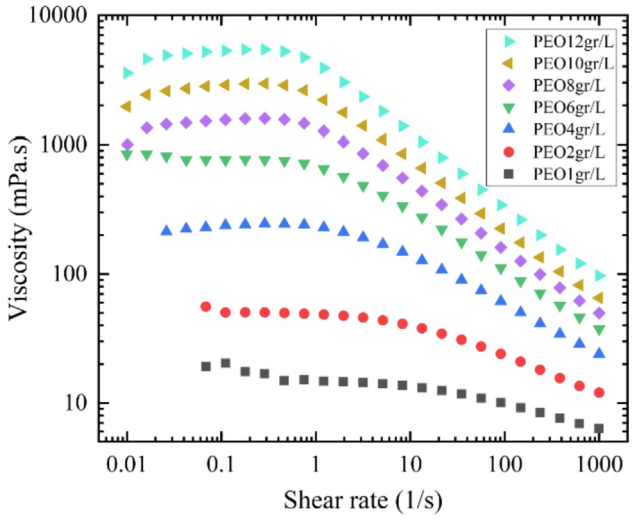

Fig. 2. Shear viscosity of the solutions containing different concentrations of PEO and 0.3 M SDS.

Using the frequency at which G' and G'' intersect, one can define a relaxation time (τ) for the system. For low polymer concentration, the intersection of G' and G'' could not be detected within our experimental range of frequency. Relaxation time was calculated by extrapolating the G' and G'' to higher frequencies. The relaxation time of our samples varied from less than 8 ms for PEO 1 gr/L to 250 ms for PEO 12 gr/L.

3.2. Spreading dynamics and interfacial instabilities

To study the spreading dynamics, we deposit a droplet of polymer-surfactant solution on the soap film and track the spreading front in time. Although the droplet and the soap film are composed of miscible liquids, the Péclet number in all experiments is orders of magnitude smaller than one. Thus the mass diffusivity could be neglected during the course of spreading. In all our experiments, the droplet's surface tension is lower than the surface tension of the soap film. Therefore, after deposition, the droplet forms a new film in the center of the soap film and spreads to the edges. This spreading area then divides into two regions (Fig. 1 top, left): a central region where the main body of the droplet rests (with radius R_c) and an advancing thin-film moving ahead (with radius R). R_c increases in time in a power-law manner with an exponent of 0.1 ± 0.02 (data are shown in SI, Fig. 4), indicating this region spreads according to Tanner's law [19,24]. Here, the capillary pressure induced by the curvature at the rim of this region drives the spreading.

In the leading region, the thickness of the film is much smaller than the central region, resembling the precursor films introduced in the previous studies [3,25]. This thin region is in direct contact with the initial soap film; thus, the surface tension gradient dominates the spreading dynamics in this region. Fig. 5 demonstrates the growth of the radius of this region (R) in time for various concentrations of PEO (4×10^6 amu). Solid data points represent spreading with a perfectly circular (stable) front, while the open symbols represent experiments in which the spreading front becomes unstable.

After deposition, the radius of the droplet first grows slowly (lag phase) then, it evolves rapidly (second phase) until it is slowed down again by the boundary effects at the edge of the container. In the lag phase, there is no clear distinction between R and Rc; therefore, the precursor film is not formed yet. This phase often occurs at time scales smaller than the relaxation time of the solutions (τ), where the system mostly represents its solid-like behavior and thus, the growth of the radius of the droplet is slower.

Power-law functions ($R \propto t^{\alpha}$) were fitted to the solid data sets (stable front) in the second region (between the dashed lines in Fig. 5 left), and exponent α is reported in the inset of Fig. 5 as a function of polymer concentration for different polymeric systems. With a good approximation, α is scattered around one. It is shown that balancing the surface tension gradient as the driving force of spreading with inertial terms in this system results in an exponent of 2/3 [19]. However, the viscosity of our polymer solutions is often considerably high and the viscous dissipation is dominant with respect to the inertial term. Since the spreading film is suspended in the air, the velocity gradient through the thickness of the film is nearly zero. Therefore, the viscous dissipation acts only along the radius of the droplet. By scaling the viscous stress with the surface tension gradient, we will have $\eta \frac{V}{R} \propto \frac{\Delta\sigma}{R}$ where η is the viscosity of the spreading liquid and $\Delta\sigma$ is the surface tension difference. This will result in $R \propto t$ thus α is equal to 1. The prefactor $\frac{\Delta\sigma}{\eta}$ has an order of magnitude of 0.1 to 0.01 m/s in our experiments. The good agreement of our scaling discussion with the experimental results of Fig. 5 (left) indicates that for the stable spreading of polymer

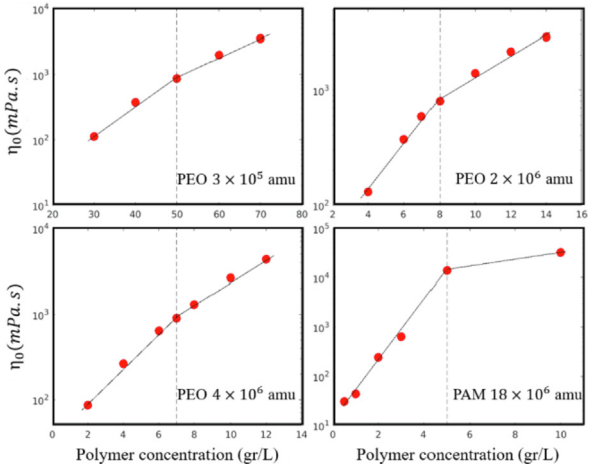

Fig. 3. Zero shear viscosity as a function of polymer concentration for different molecular weights of PEO and PAM. All the solutions contained 0.3 M SDS. The dashed lines indicate the crossover concentration.

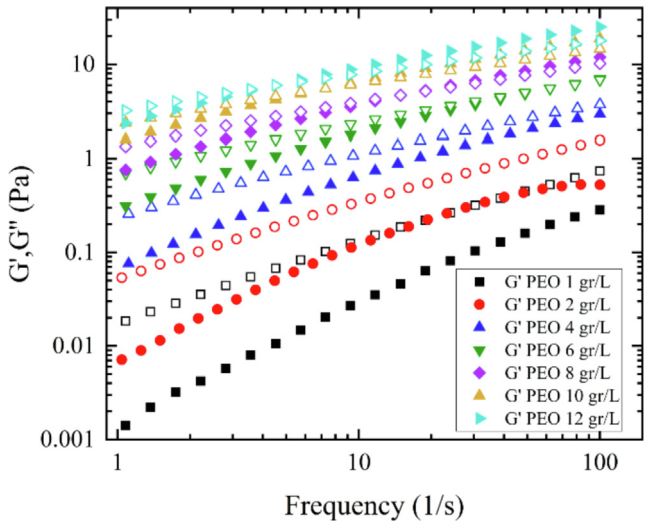

Fig. 4. Frequency sweep test of solutions containing 0.3 M SDS and various concentrations of PEO 4 × 10^6 amu. Solid symbols represent the elastic modulus and open symbols of the same shape show related loss modulus.

solutions, the capillary driving force is balanced by the viscous dissipation in the growing thin film.

For PEO concentrations of 8 gr/L and higher, the spreading front is no longer stable, and after deposition of the drop, azimuthal undulations emerge on the leading edge (Fig. 1 right). This daisy shape front grows until it reaches the boundaries. The instability also occurs for different molecular weights of PEO and PAM and different combinations of polymer-surfactants when the polymer concentration is above a critical level. This critical concentration decreases by increasing the molecular weight of the polymer, and it is 8 for PEO of 4 × 10^6, 2 × 10^6, and 50 gr/L for PEO of 3 × 10^5 amu and 5 gr/L for PAM 18 × 10^6. Strikingly, these concentrations coincide precisely with the entanglement concentration (C_e) introduced in the previous section.

In order to check if the instability has a viscous origin or initiates due to shear thinning of the solutions, we have performed spreading experiments with a droplet of 30 wt% ALS in water on a soap film of 0.01 M SDS. The ALS solution has a zero shear viscosity of 42.9 Pa.s, high above the zero shear viscosity for the onset of instability in all our polymer samples, and shows a shear-thinning behavior similar to the polymer solutions. The spreading front of the ALS droplet remains perfectly stable (Fig. 7SI) with a spreading exponent of α = 1.1, indicating that instability is not derived by the viscosity or shear thinning. These observations suggest that the elastic properties of the liquid should govern the instability since, above the entanglement concentration, the elastic contribution dominates, owing to the liquid acting as a network of entangled springs.

Looking back at Fig. 5 (left), one can notice that the spreading of the droplets takes place in time scales comparable to the relaxation time of each sample, especially for the higher concentrations of polymer. Therefore, we expect the elastic response of the polymeric solution would be dominant in the spreading dynamics at high polymer concentrations. Balancing the elastic energy with the surface energy in a stretching liquid film gives a capillary-elastic length scale:

$$l_{c-el} \quad \frac{\sigma}{G'(\omega)}$$

with an order of magnitude between 1.5 mm and 28.7 m in our system. Since G' increases by increasing the frequency of applied deformations (ω), G' decreases in time and l_{c-el} increases when the polymer relaxes during the course of spreading. When the droplet radius during the spreading grows at a lower rate with respect to l_{c-el} , the spreading front can stay stable. On the other hand, if the growth of the spreading edge exceeds the growth of l_{c-el}, the leading edge becomes unstable. In Fig. 5 (right), we plot the dimensionless radius of spreading (R/ l_{c-el}) as a function of dimensionless time (t/τ). The solid symbols represent stable spreading, while the hollow symbols show unstable samples. The inset of Fig. 5 (right) shows the same plot for similar droplets deposited on a soap film of 0.005 M SDS, which has a higher initial surface tension than 0.1 M SDS solution. In both systems, R/l_{c-el} is an excellent predictor of the onset of instability. For the soap film of 0.005 M SDS, instabilities could be observed at slightly lower polymer concentration (6 gr/L).

When R grows faster than l_{c-el}, the system is susceptible to disturbances; thereby, any perturbation amplifies and grows into petals in the leading front. In the case of R/l_{c-el} < 1, on the other hand, small perturbations are damped, and the front remains circular. However, adding a minute amount of microparticles to the polymer solution triggers large long-lived disturbances in the leading front, promoting instability at concentrations lower than the critical concentrations (See SI, Fig. 8).

To investigate the effect of surfactant type on the onset of instability, we performed experiments with three different surfactants (0.3 M SDS, 0.5 M ALS, 8 mM AOT) in PEO (4 × 10^6 amu) solutions. The critical concentration for the onset of instability for the systems containing SDS and ALS were relatively close with 8 and 7 gr/L, respectively. Surprisingly for the systems of PEO-AOT, instability is observed at a much higher critical concentration of 18 gr/L. In addition, the viscosity of solutions of PEO-AOT is significantly lower than their counterpart with the same concentration of PEO and different surfactants (See Fig. 5 SI). The difference in the critical concentration for different surfactant systems lies in their different molecular structure and their interactions with the polymers in the solution. ALS and SDS have similar hydrophobic tails, and they interact with the hydrophobic portions of PEO similarly. The formation of mutual micelles between polymer strands acts as linkers and promotes the entanglement of strands [26]. AOT with a double tail, on the other hand, has a very different molecular structure. Because of its large molecular structure, AOT cannot readily form micelles to form linkers between the strands of the

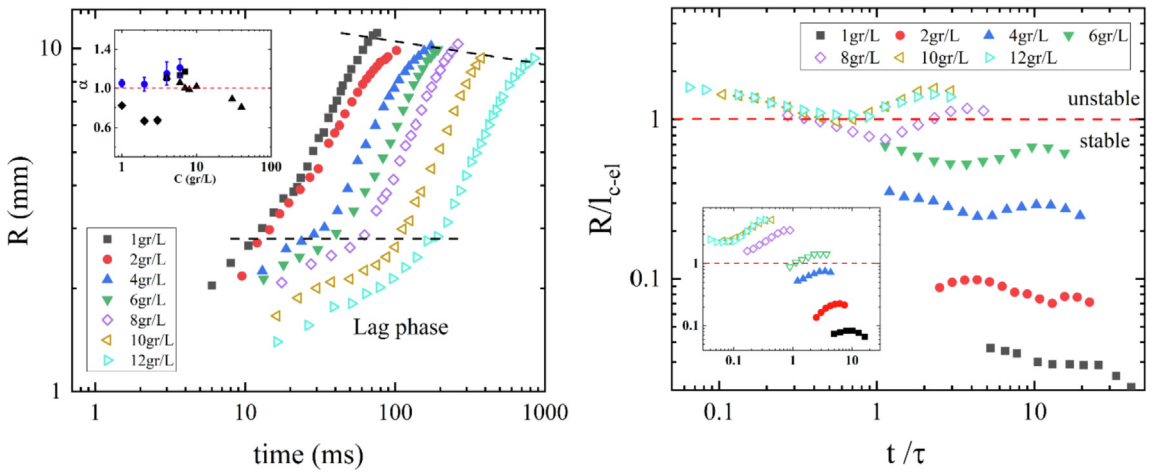

Fig. 5. (left) Radius of the advancing edge as a function of time for different concentrations of the polymer. Numbers in the legend indicate concentrations of PEO with 4×10^6 *amu*. Solid symbols represent stable spreading front while open symbols refer to unstable spreading fronts. Inset: exponent α is shown as a function of polymer concentration for the stable spreading of four polymer -SDS solutions: (● PEO 4×10^6 ■ PEO 2×10^6 ▲ PEO 3×10^5 ◆PAM 18×10^6 – data points for PEO 4×10^6 is highlighted in blue) Error bars for α values illustrated for spreading of PEO 4×10^6 based on two series of spreading measurements. For the rest of the data points, the error bar is smaller than ± 0.1. (Right) R/l_{c-el} as a function of dimensionless time for various concentrations of PEO (4×10^6 amu) and 0.3 M SDS deposited on the soap film of 0.01 M SDS. Hollow symbols represent the unstable spreading experiments and the solid ones are the stable spreading. Inset: the same plot for an experiment with a soap film of 0.005 M SDS.

polymer; thus, it impedes the entanglement. Therefore, the structure of the surfactant can affect the onset of the instability by affecting the entanglement concentrations.

4. Conclusion

We studied the spreading dynamics of multicomponent droplets containing polymers and surfactants on a soap film and observed a novel interfacial instability during spreading at high concentrations of polymer. We found that the instability has an elastic origin and is governed by the interplay between the surface tension as the driving force of spreading and the elastic properties of the polymer solution responsible for the destabilization of the spreading front. A capillary-elastic length was introduced. Comparing the growth rate of mentioned capillary-elastic length to the growth rate of the radius of spreading droplet determined the onset of instability. The general spreading dynamics of the stable front below the critical concentration were discussed. The radius of the stable spreading front grew linearly in time and was explained by a viscous scaling argument.

The spreading of droplets on solid or liquid substrates has been extensively studied in the past [5,27,28] and it is well known that solid or liquid boundaries can significantly influence the spreading behavior of liquids. The specific geometry that we have used in this work has allowed us to study the spreading behavior of multicomponent liquids in the absence of solid boundaries. We observed that in this scenario, the elastic response of polymer-surfactant solution strongly influences the spreading behavior resulting in a novel interfacial instability. These results inspire more fundamental and theoretical studies of this novel instability and free surface multi-component systems in general for applications from 2D stretching of polymer films to coating by multi-component droplets or even indirect rheological probing of complex liquids.

Declaration of Competing Interest

The authors declare that they have no known competing financial interests or personal relationships that could have appeared to influence the work reported in this paper.

Acknowledgement

We acknowledge fruitful discussions with J. Bico and E. Reyssat. M.H. acknowledges funding from the Netherlands Organization for Scientific Research through NWO-VIDI grant No. 680-47-548/983.

Appendix A. Supplementary data

Supplementary data to this article can be found online at https://doi.org/10.1016/j.jcis.2021.12.168.

References

[1] V. Bergeron, D. Bonn, J.Y. Martin, L. Vovelle, Controlling droplet deposition with polymer additives, Nature 405 (6788) (2000) 772–775.
[2] D.P. Gaver, J.B. Grotberg, The dynamics of a localized surfactant on a thin film, J. Fluid Mech. 213 (1990) 127–148.
[3] F. Heslot, N. Fraysse, A.M. Cazabat, Molecular layering in the spreading of wetting liquid drops, Nature 338 (6217) (1989) 640–642.
[4] D.A. Bolleddula, A. Berchielli, A. Aliseda, Impact of a heterogeneous liquid droplet on a dry surface: application to the pharmaceutical industry, Adv. Colloid Interface Sci. 159 (2010) 144–159.
[5] P.-G. Gennes, F. Brochard-Wyart, D. Quéré, A. Reisinger, B. Widom, Capillarity and Wetting Phenomena: Drops, Bubbles, Pearls, Waves, Phys. Today 57 (2004) 66–67.
[6] D.W. Camp, J.C. Berg, The spreading of oil on water in the surface-tension regime, J. Fluid Mech. 184 (1987) 445–462.
[7] S. Yamani et al., Spectral Universality of Elastoinertial Turbulence, Phys. Rev. Lett. 127 (2021) 74501.
[8] P.G. De Gennes, Dynamics of Entangled Polymer Solutions. I. The Rouse Model, Macromolecules 9 (4) (1976) 587–593.
[9] S. Seiffert, J. Sprakel, Physical chemistry of supramolecular polymer networks, Chem. Soc. Rev. 41 (2) (2012) 909–930.
[10] L. Keiser, H. Bense, P. Colinet, J. Bico, E. Reyssat, Marangoni Bursting : Evaporation-Induced Emulsification of Binary Mixtures on a Liquid Layer, Phys. Rev. Lett. 074504 (2017) 1–5.
[11] S.M. Troian, X.L. Wu, S.A. Safran, Fingering instability in thin wetting films, Phys. Rev. Lett. 62 (1989) 1496–1499.
[12] M. Habibi, Y. Rahmani, D. Bonn, N.M. Ribe, Buckling of Liquid Columns, Phys. Rev. Lett. 104 (2010) 74301.
[13] B. Keshavarz, E.C. Houze, J.R. Moore, M.R. Koerner, G.H. McKinley, Ligament Mediated Fragmentation of Viscoelastic Liquids, Phys. Rev. Lett. 117 (2016) 154502.
[14] E. Villermaux, B. Bossa, Single-drop fragmentation determines size distribution of raindrops, Nat. Phys. 5 (2009) 697–702.
[15] J.W. Hoyt, J.J. Taylor, C.D. Runge, The structure of jets of water and polymer solution in air, J. Fluid Mech. 63 (1974) 635–640.
[16] A. Deblais, K.P. Velikov, D. Bonn, Pearling Instabilities of a Viscoelastic Thread, Phys. Rev. Lett. 120 (2018) 194501.

[17] R. Sattler, C. Wagner, J. Eggers, Blistering Pattern and Formation of Nanofibers in Capillary Thinning of Polymer Solutions, Phys. Rev. Lett. 100 (2008) 164502.
[18] C. Clasen, J. Bico, V.M. Entov, G.H. Mckinley, 'Gobbling drops': the jetting–dripping transition in flows of polymer solutions, J. Fluid Mech. 636 (2009) 5–40.
[19] M. Motaghian, R. Shirsavar, M. Erfanifam, M. Sabouhi, E. van der Linden, H.A. Stone, D. Bonn, M. Habibi, Rapid Spreading of a Droplet on a Thin Soap Film, Langmuir 35 (46) (2019) 14855–14860.
[20] Feldman, D. The theory of polymer dynamics, by M. Doi and S. F. Edwards, the Clarendon Press, Oxford University Press, New York, 1986, 391 pp. Price: $78.50. *J. Polym. Sci. Part C Polym. Lett.* **27**, 239–240 (1989).
[21] A. Deblais, A.C. Maggs, D. Bonn, S. Woutersen, Phase Separation by Entanglement of Active Polymerlike Worms, Phys. Rev. Lett. 124 (2020) 208006.
[22] K.W. Ebagninin, A. Benchabane, K. Bekkour, Rheological characterization of poly(ethylene oxide) solutions of different molecular weights, J. Colloid Interface Sci. 336 (2009) 360–367.
[23] A. Fall, D. Bonn, Shear thickening of Laponite suspensions with poly(ethylene oxide), Soft Matter 8 (17) (2012) 4645, https://doi.org/10.1039/c2sm07089h.
[24] L.H. Tanner, The spreading of silicone oil drops on horizontal surfaces, J. Phys. D. Appl. Phys. 12 (9) (1979) 1473–1484.
[25] F. Heslot, A.M. Cazabat, P. Levinson, Dynamics of wetting of tiny drops: Ellipsometric study of the late stages of spreading, Phys. Rev. Lett. 62 (1989) 1286–1289.
[26] P. Dastyar, M.S. Salehi, B. Firoozabadi, H. Afshin, Influences of Polymer-Surfactant Interaction on the Drop Formation Process: An Experimental Study, Langmuir 37 (3) (2021) 1025–1036.
[27] J.G.E.M. Fraaije, A.M. Cazabat, Dynamics of spreading on a liquid substrate, J. Colloid Interface Sci. 133 (2) (1989) 452–460.
[28] O.E. Jensen, J.B. Grotberg, Insoluble surfactant spreading on a thin viscous film: Shock evolution and film rupture, J. Fluid Mech. 240 (1992) 259–288.